Investigations on the Effects of DC Voltage Control on Inertia Provision in HVDC Converter Stations

Ying Pang, Juan-Carlos Gonzalez, Filipe Perez, Abdelkrim Benchaib, Kosei Shinoda, Agusti Egea Alvarez

Investigations on the Effects of DC Voltage Control on Inertia Provision in HVDC Converter Stations

Ying Pang, Juan-Carlos Gonzalez
Filipe Perez, Abdelkrim Benchaib, Kosei Shinoda
SuperGrid Institute
Villeurbanne, France
{ying.pang, juan-carlos.gonzalez}@supergrid-institute.com

Agusti Egea Alvarez
Electronic and Electrical engineering department
University of Strathclyde
Glasgow, UK
agusti.egea@strach.ac.uk

***Abstract*— To mitigate the low-inertia challenges in future power-electronics-dominated grid, grid-forming control with virtual inertia has been proposed to grid-connected power converters, including the converter stations in high-voltage-direct-current (HVDC) transmissions, where DC voltage also needs to be tightly controlled. This paper first demonstrates that if there is only one station in charge of DC voltage control, this station cannot provide any real inertia power during frequency events but instead adversely produces a small equivalent negative inertia. Then, an improved grid-forming control with enhanced DC voltage droop control that has been recently proposed is examined in same perspective. It is found that with this novel control real inertia power can be delivered while poses negligible disturbances on the DC voltage, rendering it an excellent control strategy to sharing inertia reserves from different AC areas without commnunications. All findings are validated in electro-magnetic simulations with MMC models of 400 sub-modules.**

***Index Terms*—Grid-forming, HVDC, Inertia, DC voltage control, DC voltage Droop Control**

I. Introduction

A comprehensive and in-depth description of the low-inertia challenges in future power grids is given in [1]. Such challenges arise from two aspects. First, the fast increase of renewable energy penetration reduces the overall system inertia since its interface to the AC grid, the power electronics converters, lack the physical rotor mass brought by the traditional synchronous machines (SMs). Second, renewable energy sources such wind and solar energy, are by nature intermittent, incurring susceptibility of active power imbalance into the AC grids. The combination of these two factors could potentially lead to high rate-of-change-of-frequency (RoCoF) or excessive frequency-nadir induced generation units disconnection , cascaded events and system splits, threatening the reliability and the resiliency of the AC grids.

To mitigate these issues, various grid-forming (GFM) controls with virtual inertia have been introduced to the grid-interfaced converters with the goal to improve frequency stability by mimicking the rotor mass of SMs [2]. In fact, the new EU and UK grid codes are starting to demand such behavior from the grid-connected converters [4][3]. HVDC converter stations, playing an increasingly important role in the future power systems, are also expected to provide such inertia power (INP) response.

However, it has been pointed out in [5] that within the HVDC converter stations, the control objective of GFM INP provision contradicts with the objective of DC voltage control (DVC) – increasing the inertia constant in GFM control slows down the power response, yet to maintain the DC voltage stability, fast power response from converter stations is required. Even though [6] studies the back-to-back converters in wind turbine, its learning is extendable to VSC-based HVDC. It points out the same conflicts between INP and DVC and both work suggest that virtual inertia and its AC frequency service have to be traded off for DC stability.

Yet, [5] only study the detrimental effects of the increased virtual inertia on DC voltage security during AC transients, such as AC faults and device connection/disconnection, without examining whether increasing the virtual inertia in the DVC station actually benefits the AC frequency stability. [6] attempts to perform such a study but it chooses a step signal in the grid frequency as the test signal, which does not directly reveal whether real INP can be provided by the DVC station. This paper first applies the constant RoCoF (C-RoCoF) test recommended by [4], which reveals that a single DVC station cannot provide any INP. Then, a second test method is introduced by applying a low-frequency sinusoidal frequency oscillation (SFO) to the grid, which thus allows analysis on the phase of converter power and it demonstrates that with a single DVC station, it tends to produce even negative inertia and thereby deteriorates frequency stability. Virtual inertia and DC stability is thus NOT a trade-off problem in this case, since reducing it benefits both frequency and DC stability.

However, these conclusions only apply to the conventional master-slave control where there is only one DVC station. In the future multi-terminal HVDC (MTDC) grids that are being planned and constructed in Europe, it is desirable to have multiple stations participating in the DC voltage droop control (DVD) since the failure of the single DVC station in master-slave control would paralyse the entire system whereas MTDC with DVD can be designed to ride-through N-1 contingency. In [7], the harmonic instability issues when combining GFM with DVD with the droop gains needed to ride through N-1

979-8-3503-9042-1/24/$31.00

contingency are studied, based on which two modifications, the phase compensator (PCom) and virtual power system stabilizer (VPSS) are introduced to resolve the issues. The paper extend the study on this improved control strategy by examining its capability of INP provision and it is found that real INP can be delivered with negligible disturbance on the DC voltage, which makes possible to share inertia reserves across different AC areas via DC interconnections if TSOs choose to do so. Then, the relationships between the INP, the droop gains and the number of terminals are also determined. All findings are verified by EMT simulations with MMC models of 400 sub-modules.

II. The Converter Under Study and the Adopted Grid-Forming Control Strategy

The understudied 3-terminal HVDC system is shown in Fig. 1. MMC models with 400 sub-modules, DC reactors, DC wide-band cable models are implemented in the EMT simulation in EMTP-rv. The AC grids can be modelled by an ideal sources representing infinite bus or a simplified grid modelled by the swing equation plus the simplified governor and turbine dynamics, which is chosen depending on the constructed study cases.

A recently proposed improved DVD plus GFM control [7] is shown in Fig. 2, which consist of four units: Active power control (APC), DVD, AC voltage control (AVC) and circulating-current suppression control (CCSC) as the MMC internal control. The APC, which also serves as the synchronization unit, is based on the Virtual Synchronous Machine (VSM) control with a PLL providing frequency information from the point of common coupling (PCC) and enabling the VSM to follow its power reference when the grid frequency deviates [8]. The AVC is realized with direct voltage modulation plus a transient damping resistor (TDR), since it has been demonstrated that this simple structure performs superior to the cascaded control with a inner current loop in providing grid strength and stability [9]. Its over-current protection [10] are not triggered during small-signal disturbances of the converter and therefore neglected in the studies in this paper. The modifications proposed in [7] is the addition of the PCom and VPSS to overcome the potential harmonic instability that can be triggered on the DC-side.

III. Inertia Response and Its Test Methods

A. C-RoCoF Test

A simplified swing equation of an SM can be seen in (1), from which it can be understood that the inertia constant H_G brought by rotor mass limits the change of speed $\dot{\omega}_G$ by relating it to active power and thereby counteracts its imbalance during transients. Based on this logic, a test method has been proposed in [4] suggesting to test the GFM device by applying a C-RoCoF (i.e., $\dot{\omega}_G = C_{RoCoF}$) to the AC grid emulator on the test bench, with a constant power response expected as in (2).

$$2H_G\dot{\omega}_G = P_m - P_e - D_G(\omega_G - \omega_{ref}) \tag{1}$$

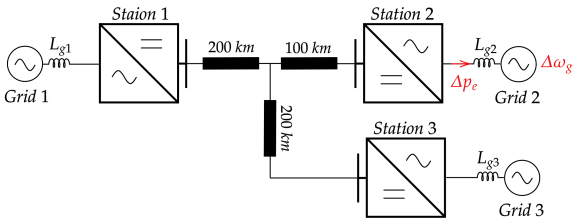

Fig. 1. The understudied 3-terminal HVDC system. To demonstrate the impact of the number of terminals, in some study cases Station 3 and all of its DC connection components are disconnected from the network to form a 2-terminal system. MMC models with 400 sub-modules are implemented for each station. DCRs and wide-band DC cable models of 525 kV are also implemented in the simulations. The grid impedance is assumed as $0.25\,p.u.$.

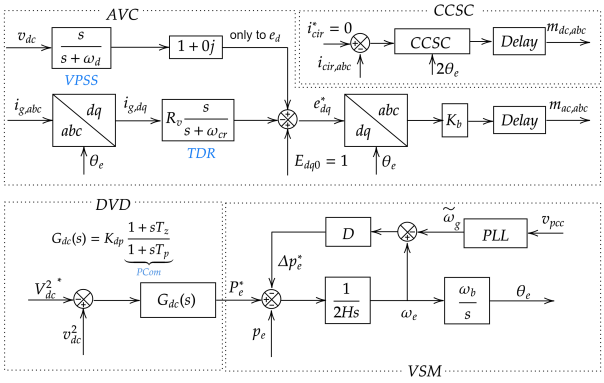

Fig. 2. Block diagram of the improved DVD plus GFM control strategy proposed in [7]. In the study case where Master-Slave control is used, the VPSS will be removed and the DVD will be replaced by PI controller for the Master Station, namely, $G_{dc}(s) = K_p + \frac{K_i}{s}$ and $G_{dc}(s) = 0$ for the Slave Stations in power mode. Other parameters used in this paper unless specifically changed: $H = 6\,s$, $D = 700$, $K_{dp} = 5\,p.u.$, $T_z = 0.8$, $T_p = 3.3 \times 10^{-4}$, $\omega_d = 10\pi\,rads/s$, $\omega_{cr} = 20\pi\,rads/s$

$$P_e = -2H_G\dot{\omega}_G = -2H_G C_{RoCoF} \tag{2}$$

B. SFO tests

A second test method used in this paper is to superimpose a small SFO on the AC grid frequency and to measure the response in the converter output power, i.e.:

$$\omega_g = \omega_{g0} + \Delta\omega_g = 2\pi[50 + \sin(0.2\pi t)] \tag{3}$$

The SFO is chosen of 0.1 Hz since the oscillations of center-of-inertia frequency typically occur in this range. This method is able to reveal the phase of the power response to an SFO, which determines whether it is truly stabilizing the frequency. In the case where true INP is provided, according to (1), the power should be leading the injected frequency disturbance by 90° if synchronization is assumed.

IV. Inertia Response tests on the Master Station

In this section, the two test methods discussed in III will be first applied to the single DVC station in the Master-Slave

configuration and reveals that not only real INP is inaccessible from this station but even negative INP can be excited.

A. The Master Station in C-RoCoF tests

For this test, Station 2 in Fig. 1 is configured as the Master Station and it performs the DVC with a PI. Station 1 and 3 are configured in constant power mode. Then a C-RoCoF of 0.5 Hz/s is introduced in Grid 2 and the active power response of Station 2 is measured and plotted in Fig. 3. In order to demonstrate the underlying logic of the C-RoCoF test, a reference case is also constructed by connecting a DC battery at the DC terminal of Station 2 and deactivating the DVC and its dynamics. It can be observed in Fig. 3 that within the reference case, the active power response to the C-RoCoF reaches a constant at the steady-state with its value exactly as predicted by (2).

However, without the DC batteries and with the DVC dynamics imposed, the power response from Station 2 reaches 0 W at the steady-state. This gives the first straightforward proof that real INP does not exist in the Master Station. Such results may not appear surprising since with all the Slave Stations in constant power mode, there is no stable energy source to provide the extra constant power. However, what the SFO tests further reveal is that the posed problem is more than just a lack of disposable DC energy. The DVC dynamics can modify the phase of the power response to an SFO in a way that it becomes adverse to frequency stability.

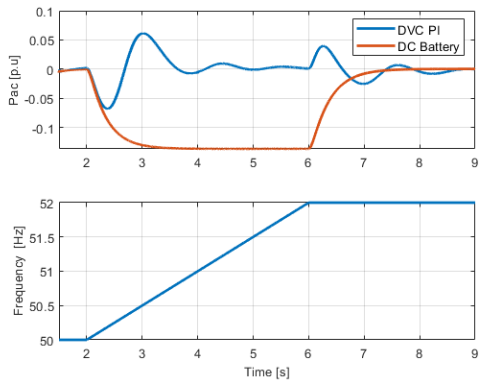

Fig. 3. The power response to a C-RoCoF from the Master Station employing a PI-based DVC in comparison to a reference case where DC batteries are connected on the DC-side with all DVC dynamics eliminated. It can be clearly observed that with the reference case the INP is reaching the expected constant value at the steady-state yet with the DVC dynamics imposed, it reaches 0 W at the steady-state.

B. The Master Station in SFO tests

In this test, the Master-Slave configuration and the reference case is identical to the one in the C-RoCoF test but with the frequency in Grid 2 being disturbed by a small sinusoidal signal as described in (3). It can be observed in Fig. 4 that with the reference case, the power response is indeed leading the injected frequency oscillation by 90° yet without the DC batteries and with the DVC dynamics imposed, the power response from Station 2 is lagging the oscillation by 90°. This implies a negative inertia behavior by which larger virtual inertia constants lead to larger negative inertia behavior and worst frequency stability. Although, it can also be seen in Fig. 4 that the magnitude of such negative inertia power response, compared to the reference case, is much smaller, which means that its frequency destabilizing effects are limited.

The mechanism of such phase modification by the DVC can be understood by a simplified model of the control in Fig. 2, in which the dynamics of TDR, VPSS are neglected since they are not active within the ultra low frequency range of grid frequency oscillation (generally below 1 Hz). Plus, the dynamics of CCSC can be neglected and the MMC can be approximated by a 2-level voltage source converter [7] for studying its LF dynamics. Then, Assuming that the VSM of Station 2 is well synchronized with the grid, (4) and sequentially (5) can be derived, from which it can be observed that the double integral dynamics formed by the DC arm capacitance (C_{dc}) and the PI integrator are what introduces the 180° phase shift to the power and thereby forms the negative inertia. Additionally, it can be deduced that if the integrator of the PI gets reduced, the phase shift will approach 90° instead and constitutes a negative damping on the frequency, which is also undesirable. The third conclusion can be drawn is that increasing the DC voltage control gains generally reduces such negative effects on the frequency stability by reducing the magnitude of the active power response.

$$G_{dc}(s)\Delta v_{dc2}^2 = G_{dc}(s)\frac{-2\Delta p_{e2}}{sC_{dc}} \approx \Delta p_{e2} + 2H\Delta\ddot{\theta}_{e2} \quad (4)$$

$$\Delta p_{e2} = \frac{-sC_{dc}}{sC_{dc}+2G_{dc}(s)}2H\Delta\ddot{\theta}_{e2} \approx \frac{-s^2C_{dc}}{2(sK_p+K_i)}2H\Delta\ddot{\theta}_{e2} \quad (5)$$

C. Load jump test in finite AC Grid

To further illustrate the effects of negative inertia, a load jump test are designed with Grid 2 rated as 1 GW instead of infinite bus and its frequency characteristics are determined by a simplified governor + turbine + inertia model as shown in Fig. 5. A sudden load jump of 0.5 GW is introduced by a constant power load modeled by a GFL converter. It can be observed in Fig. 6 that a larger inertia constant indeed leads to a slightly worst frequency nadir in Grid 2 and a far worst the DC voltage nadir at the same time, which matches the negative but limited inertia measured by the SFO tests and drives to the conclusion that increase the virtual inertia in a single Master Station brings only deterioration of stability, on both AC and DC side.

V. Inertia Provision with the Enhanced DC Voltage Droop Control

In this section, similar tests described in Section V will be applied to a 2 or 3 terminal system with each station participating the DVD with the control strategy illustrated in Fig. 2. It is found that real INP is made possible with

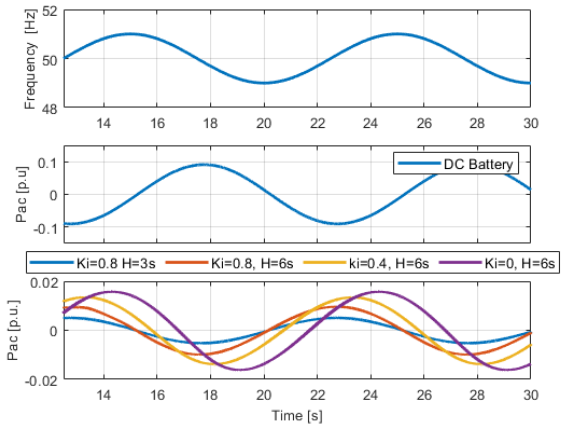

Fig. 4. The power response to a SFO from the Master Station employing a PI-based DVC in comparison to a reference case where DC batteries are connected on the DC-side with all DVC dynamics eliminated. It can be seen that with the reference case the INP is leading the SFO by 90° as expected yet with the DVC dynamics imposed, the power response is lagging the frequency disturbance by 90°, suggesting that it exhibits a negative inertia behavior. Increasing the virtual inertia leads to stronger negative inertia effects and reducing the integrator in the PI leads to a mixture of negative inertia and negative frequency damping.

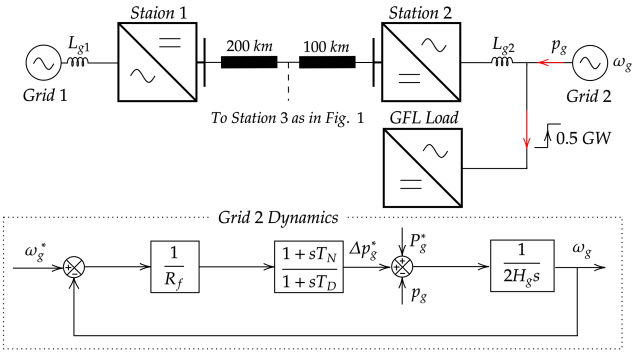

Fig. 5. The load jump test setup by performing a 0.5 GW load increase from a GFL converter connected to Grid 2, which is replaced by a finite grid rated at 1 GVA with a simplified inertia plus primary control dynamics. $R_f = 0.04$; $T_N = 1$; $T_N = 6$; $H_g = 6.175$.

this control by dynamically dispatching power from other AC areas with negligible disturbances introduced to the DC voltage. Numerical relationships between the effective inertia, the droop gains and the number of terminals are also analysed and validated by simulations.

A. Inertia power response in C-RoCoF tests

With the same control strategy depicted in Fig. 2 implemented in all stations, C-RoCoF is again applied to Grid 2 and the power response of Station 2 is captured in Fig. 7. It can be seen that a constant power is reached at the steady-state in this case, implying that the INP is delivered with this control.

Next, to understand the effective inertia formed by dispatching power from other AC areas, a generalized analysis for

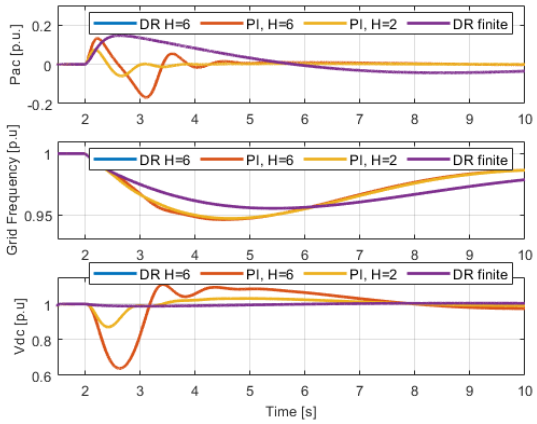

Fig. 6. The simulation results of the load jump test. It can be seen that with a single DVC station, increasing the virtual inertia leads to a slightly WORST frequency nadir due the increased negative inertia effects, and a much worst DC voltage nadir as well. Whereas with the improved droop control, frequency nadir is improved with negligible disturbance on the DC voltage. It can also be observed that whether Grid 1 and 3 are infinite bus (blue) or not (purple), has no impact on the inertia formed at Station 2.

a N-terminal MTDC is performed by describing the system approaching the quasi-steady-state during C-RoCoF or LF-SFO. When the active power of the i^{th} Station reaches a quasi-steady-state, it is well synchronized with the i^{th} grid and the rest of the N-1 stations follow their own references generated by the DC voltage deviation, which gives (6) and (7) based on Fig. 2. Then, considering the losses in the system has negligible effects on its dynamics, another two boundary conditions can be set as (8). Combining (6), (6) and (8), gives (9) and (10). which means that the magnitude of the INP is the expected value defined by H_i scaled by the DC droop gain relations.The second half of (9) is derived assuming that the same PCom is applied to all stations, and it is valid during both C-RoCoF and LF-SFO. (9) and (10) is then verified in the simulation results in Fig. 7 – in the 2-terminal case the effective inertia is $\frac{1}{2}H$ and in the 3-terminal case it is $\frac{2}{3}H$ and the DC voltage deviation also scales down according to (10) as the number of terminals increases.

$$2G_{dc,i}(s)\Delta v_{dc,i} \approx \Delta p_{e,i} + 2H_i\Delta\ddot{\theta}_{e,i} \tag{6}$$

$$2G_{dc,j}(s)\Delta v_{dc,j} = \Delta p_{e,j}, j \in [1, N], j \neq i \tag{7}$$

$$\sum_{j=1}^{N} p_{e,j} = 0, \quad \Delta v_{dc,j} = \Delta v_{dc,i} \tag{8}$$

$$\begin{aligned}\Delta p_{e,i} &= -\frac{\sum_{j=1}^{j=N} G_{dc,j}(s) - G_{dc,i}(s)}{\sum_{j=1}^{j=N} G_{dc,j}(s)} 2H_i\Delta\ddot{\theta}_{e,i} \\ &= -\frac{\sum_{j=1}^{j=N} K_{dp,j} - K_{dp,i}}{\sum_{j=1}^{j=N} K_{dp,j}} 2H_i\Delta\ddot{\theta}_{e,i}\end{aligned} \tag{9}$$

$$\Delta v_{dc} = \frac{H_i \Delta \ddot{\theta}_{e,i}}{\sum_{j=1}^{j=N} G_{dc,j}(s)} \tag{10}$$

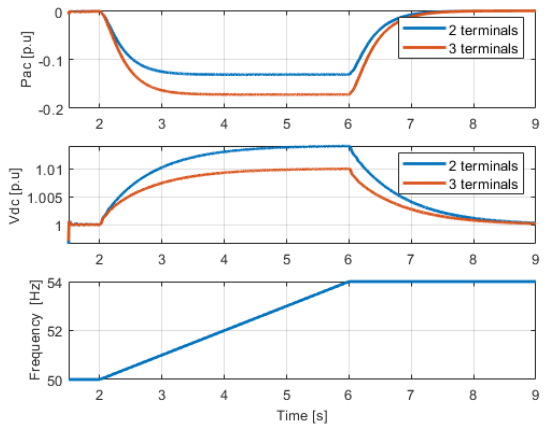

Fig. 7. The simulation results of C-RoCoF test with the improved DVD. Real INP is formed by dispatching power from other AC grids via DC voltage deviations. Given that $H = 6s$, $C_{RoCoF} = 0.02\,p.u./s$ and $K_{dp} = 5\,p.u.$, (9) and (10) are also verified by the simulations.

B. Inertia power response in Sinusoidal frequency oscillation Tests

SFO is applied again to Grid 2 and the active power response of Station 2 is depicted in Fig. 8, from which it can be observed that its phase is leading the SFO by 90°, namely, the correct phase of INP. Plus, its magnitude and the deviation of DC voltage also match the prediction by (9) and (10).

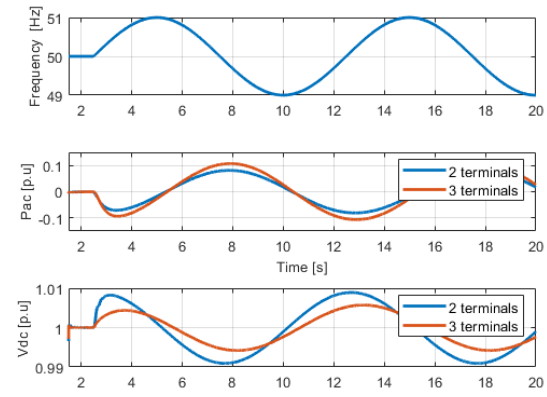

Fig. 8. The simulation results of the SFO tests with the improved DVD. The phase of the INP is correctly leading the SFO by 90°.

C. Load jump test in finite AC Grid

At last, the improved control is also tested in a load jump test with the same configuration as in Fig. 5 and compared to the results obtained by the single U-station, where the improvement on frequency nadir in Grid 2 is clearly visible while the DC voltage disturbance is negligible. Additionally, same tests are repeated with Grid 1 and 3 also being finite AC grids with the same dynamics as Grid 2 and the obtained results are identical, since Station 1 and 3 are still able to followed their power references generated by DC voltage deviation despite of the frequency variations in their AC areas.

VI. Conclusions and Future Works

This paper has demonstrated that if there is only one DVC station in a HVDC system, such as the Master Station in a Master-Slave control configuration, then applying GFM control to this station cannot improve AC frequency stability. On the contrary, increasing the virtual inertia in this station brings increased negative inertia effects, or a combination of negative inertia and negative frequency damping effects, which deteriorates the frequency stability and the DC voltage stability at the same time. An improved DC voltage droop control in combination with GFM resolves this issue by dispatching power from other AC areas to form the inertia response, while introducing negligible disturbances to the DC voltage, which makes it a good control candidate to share inertia reserves from different AC areas.

Acknowledgement

This work is supported by the HVDC-WISE project financed by European Union's Horizon Europe programme under agreement 101075424.

References

[1] F. Milano, F. Dörfler, G. Hug, D. J. Hill and G. Verbič, "Foundations and Challenges of Low-Inertia Systems (Invited Paper)," *2018 Power Systems Computation Conference (PSCC)*, Dublin, Ireland, 2018, pp. 1-25.

[2] R. Rosso, X. Wang, M. Liserre, X. Lu and S. Engelken, "Grid-Forming Converters: Control Approaches, Grid-Synchronization, and Future Trends—A Review," in *IEEE Open Journal of Industry Applications*, vol. 2, pp. 93-109, 2021.

[3] Grid forming behaviour of HVDC systems and DC-connected PPMs. Supplement to VDEAR-N 4131 for dynamic frequency/active power behaviour and dynamic voltage control without reactive current specification.

[4] GC0137: Minimum Specification Required for Provision of GB Grid Forming (GBGF) Capability, National Grid ESO, Feb., 2022.

[5] A. Abdalrahman, Y. -J. Häfner, M. K. Sahu, K. K. Nayak and A. Nami, "Grid Forming Control for HVDC Systems: Opportunities and Challenges," *2022 24th European Conference on Power Electronics and Applications (EPE'22 ECCE Europe)*, Hanover, Germany, 2022, pp. P.1-P.10.

[6] C. Henderson, D. Vozikis, D. Holliday, X. Bian, and A. Egea-Àlvarez, "Assessment of Grid-Connected Wind Turbines with an Inertia Response by Considering Internal Dynamics," *Energies*, vol. 13, no. 5, p. 1038, Feb. 2020.

[7] Y. Pang, A. Egea-Alvarez, J. C. Gonzalez-Torres, K. Shinoda, F. Perez and A. Benchaib, "DC Voltage Stability Analysis and Enhancement for Grid-Forming-Based MTDC Systems," in IEEE Transactions on Power Electronics, Early Access, Apr. 2024.

[8] T. Qoria, E. Rokrok, A. Bruyere, B. François and X. Guillaud, "A PLL-Free Grid-Forming Control With Decoupled Functionalities for High-Power Transmission System Applications," in *IEEE Access*, vol. 8, pp. 197363-197378, 2020, doi: 10.1109/ACCESS.2020.3034149.

[9] Lamrani, Yahya; Colas, Frédéric; Van Cutsem, Thierry; Cardozo, Carmen; Prevost, Thibault; Guillaud, Xavier (2023). A Comparative Study of Grid-Forming Controls and their Effects on Small-Signal Stability. *TechRxiv*. Preprint. https://doi.org/10.36227/techrxiv.22006310.v2

[10] H. Wu and X. Wang, "Control of Grid-Forming VSCs: A Perspective of Adaptive Fast/Slow Internal Voltage Source," in *IEEE Transactions on Power Electronics*, vol. 38, no. 8, pp. 10151-10169, Aug. 2023, doi: 10.1109/TPEL.2023.3268374.